Wang, H., Lühr, H., Häusler, K., Ritter, P. (2011): Effect of subauroral polarization streams on the thermosphere: A statistical study. - Journal of Geophysical Research, 116, A03312

DOI: 10.1029/2010JA016236

Effect of subauroral polarization streams on the thermosphere: A statistical study

Hui Wang,[1,2] Hermann Lühr,[3] Kathrin Häusler,[3] and Patricia Ritter[3]

Received 22 October 2010; revised 2 December 2010; accepted 21 December 2010; published 9 March 2011.

[1] Using 2 years of coordinated CHAMP and DMSP observations we have investigated for the first time the relationship between subauroral polarization streams (SAPS), ionospheric Hall current (electrojet), upper thermospheric zonal wind, and mass density at subauroral regions in the dusk and premidnight sectors, separately for both hemispheres. For comparison, we have also analyzed the same parameters as a function of magnetic latitude (30°–80° magnetic latitude) during non-SAPS periods. During periods of non-SAPS, the neutral wind exhibits similar features as during SAPS events in the dusk to premidnight sector, streaming westward in the same direction as the plasma drift. Both neutral and plasma velocities peak at the same latitude regardless of SAPS occurrence. For higher geomagnetic activity both velocities are faster and the peaks shift equatorward. During non-SAPS periods, the ratio between plasma and neutral wind velocity is on average 2.75 ± 0.4 in both hemispheres irrespective of geomagnetic activity. The neutral wind during SAPS events gets enhanced by a factor of 1.5/1.2 for $Kp < 4$ and 1.3/1.9 for $Kp \geq 4$ in the Northern/Southern Hemisphere, respectively, as compared to non-SAPS time. The velocity difference between SAPS and neutral wind is also larger during SAPS period than during non-SAPS period, and the difference tends to increase with increasing geomagnetic activity. The peak latitude of the eastward auroral electrojet appears 1.5° poleward of the plasma drift during SAPS events, confirming the formation of SAPS equatorward of the high-conductivity channel. These SAPS-induced large winds can heat the upper thermosphere. As a result we observe a 10% enhanced mass density at 400 km altitude with respect to periods without SAPS. In addition a density anomaly peak occurs collocated with the SAPS, displaced from the electrojet peak. We regard this as an indication for efficient thermospheric heating by ion neutral friction.

Citation: Wang, H., H. Lühr, K. Häusler, and P. Ritter (2011), Effect of subauroral polarization streams on the thermosphere: A statistical study, *J. Geophys. Res.*, *116*, A03312, doi:10.1029/2010JA016236.

1. Introduction

[2] The thermosphere and ionosphere are tightly coupled together due to the partially ionized upper atmosphere. The thermospheric neutral winds, the ionospheric electric field and current systems have close but complicated relationship with each other (see a review by *Richmond* [1989]). This relationship is difficult to describe, especially at middle and high latitudes, where particles are sensitive to the strongly varying electric field distribution while neutrals are controlled by both electrodynamic and hydrodynamic processes.

[3] The electric field can affect the neutrals distribution through electric current in two ways: Ampere force and Joule heating. Ampere force, also called ion drag, can work on neutrals through ion-neutral collisions. The modification of the neutrals motions can cause a change of the neutral pressure distribution, thus modifying the wind distribution. Joule heating can change the neutral temperature and induce pressure gradients, finally affecting the wind distribution. Ampere force above 125 km is thought to accelerate the neutral wind toward the $\vec{E} \times \vec{B}/B^2$ velocity, or decelerate it through the flywheel effect [*Banks*, 1972]. Some studies [e.g., *Thayer et al.*, 1987; *Emmert et al.*, 2006] found that both plasma drift and neutral wind respond in the same way to the interplanetary magnetic field (IMF), but studies from *McCormac and Smith* [1984] and *Lühr et al.* [2007b] did not resemble in all cases the tight relation between the expected plasma drift and the reported neutral wind at high latitudes. Joule heating above 125 km together with the Coriolis force drive neutral wind equatorward and westward. On the other hand, the disturbance dynamo electric

[1]Department of Space Physics, School of Electronic Informatics, Wuhan University, Hubei, China.
[2]Also at State Key Laboratory of Space Weather, Chinese Academy of Sciences, Beijing, China.
[3]Helmholtz Centre Potsdam, GFZ German Research Center for Geosciences, Potsdam, Germany.

0148-0227/11/2010JA016236

field generated by wind, can deflect the plasma drift at middle and low latitudes toward westward in all local times [*Heelis and Coley*, 1992]. It is important to understand the relationship among these electrodynamics parameters.

[4] The question we want to address in the present paper is how strong is the effect of subauroral polarization streams (SAPS) on the neutral wind in the subauroral region. This investigation has not yet been made. It will help to provide new knowledge for our understanding of the thermosphere-ionosphere coupling system.

[5] SAPS are one of the interesting and important features at subauroral latitudes. The term SAPS was introduced by *Foster and Burke* [2002] to encompass two different phenomena. One is the polarization jets (PJ) [*Galperin et al.*, 1974] or subauroral ion drifts (SAIDS) [*Spiro et al.*, 1979], characterized by more intense and latitudinally more confined plasma flow. The other is described by *Yeh et al.* [1991], featured as larger latitudinal extent and longer duration of plasma flow. SAPS have been extensively investigated for a long time from satellites and radars as well as by magnetospheric simulations [e.g., *Galperin et al.*, 1974; *Smiddy et al.*, 1977; *Spiro et al.*, 1979; *Yeh et al.*, 1991; *Anderson et al.*, 1991, 1993, 2001; *Burke et al.*, 1998; *Rowland and Wygant*, 1998; *Wygant et al.*, 1998; *Fejer and Scherliess*, 1998; *Scherliess and Fejer*, 1998; *Ridley and Liemohn*, 2002; *Foster and Vo*, 2002; *Liemohn et al.*, 2005; *Zheng et al.*, 2008]. They are rapid westward (sunward) plasma flows located equatorward of the auroral oval and are found predominantly in the dusk and premidnight sectors (1600 to 2400 magnetic local time, MLT). They can last 30 min to 3 h. SAPS velocity can be affected by both the convection electric field and the subauroral ionospheric conductivity [*Wang et al.*, 2008].

[6] The thermospheric wind has been studied extensively with observations from optical Fabry-Perot interferometer (FPI) [e.g., *Coley et al.*, 1994; *Emmert et al.*, 2001; *Meriwether et al.*, 2008], ground-based incoherent scatter radar observations [e.g., *Brekke et al.*, 1974, 1994; *Zhang et al.*, 2004], satellite instrument such as DE2 (Dynamics Explorer 2) [e.g., *Rees et al.*, 1983; *Thayer et al.*, 1987], as well as from thermospheric simulations [e.g., *Hedin et al.*, 1996; *Fejer et al.*, 2002; *Deng and Ridley*, 2006]. Recently the thermospheric wind has been derived from the cross-track acceleration measurements on board CHAMP by means of a newly developed algorithm (for full details of the processing approach the reader is referred to *Doornbos et al.* [2010]). Various papers have been published by using these CHAMP accelerometer analysis data [e.g., *Liu et al.*, 2006; *Lühr et al.*, 2007a, 2007b; *Häusler et al.*, 2007; *Ritter et al.*, 2010]. This paper for the first time examines the possible relationship between SAPS, ionospheric currents and neutral winds in a statistical way.

[7] In section 2, we briefly describe the method of data processing. In section 3, the statistical results are presented. In section 4, we compare the results with previous reports and offer explanations for the results.

2. Data Set and Processing Approach

2.1. CHAMP Zonal Wind and Hall Current

[8] CHAMP was launched on 15 July 2000 into a near-polar (83.7° inclination) orbit with an initial altitude of ~450 km [*Reigber et al.*, 2002]. The average altitude of CHAMP during the years of 2002 and 2003 is around 400 km. It precesses 1 h in local time every 11 days, thus covering all local times within 130 days.

[9] The thermospheric zonal wind is derived from the Space Three-axis Accelerometer for Research Missions (STAR) acceleration measurements on board CHAMP. Details of the method of deriving thermospheric zonal wind from the cross-track axis acceleration measurements are given by *Doornbos et al.* [2010]. The accuracy of wind measurements is about ± 10 m/s. SAPS stream westward mainly along the auroral oval. To ensure a certain alignment of the CHAMP cross-track direction with the SAPS, only results from CHAMP passes are considered where the angles between orbit track and oval is larger than 45°. This orbit selection method has been used and described in the statistical study on field-aligned currents [*Wang et al.*, 2005]. The thermospheric wind analysis has been organized in magnetic coordinates because of the strong geomagnetic forcing by plasma shift. The magnetic coordinates are based on the Apex systems as described by *Richmond et al.* [2003].

[10] The ionospheric Hall currents, more precise, the source free current components, are determined from the Overhauser Magnetometer (OVM) scalar magnetic field measurements on board CHAMP. The resolution of the magnetic field measurement is 0.1 nT. The Hall current is approximated by a series of auroral oval line currents, separated by 1 degree, which are placed in the ionospheric E region at a height of 115 km. The technique of determining the current strength of each line by inverting the variations in total magnetic field has been developed by *Olsen* [1996]. *Moretto et al.* [2002] has applied this method later to Ørsted data. The reliability of this approach has been demonstrated in a statistical study where current density estimates from CHAMP were directly compared with independent determinations from ground [*Ritter et al.*, 2004]. In the considered time sector, evening to premidnight, the determined currents represent well the auroral electrojet.

2.2. DMSP Plasma Velocity

[11] The DMSP satellites sample polar regions at ~835 km altitude along orbits of fixed local times. The orbital period is approximately 100 minutes. One of the satellites (F13) has a near dawn-dusk orbit and two (F14, F15) have dayside-nightside MLT orbits. The ion drift velocities in the horizontal and vertical directions perpendicular to the satellite track are derived from the ion drift meter (IDM) data [*Rich and Hairston*, 1994]. The DMSP electron spectrometers (SSJ/4) instruments monitor the energy flux of electrons and ions in the range of 30 eV to 30 keV that precipitate from the Earth's magnetosphere [*Hardy et al.*, 1984]. *Robinson et al.* [1987] have described the relationship relating the energy flux and the average energy of the electrons with the height-integrated ionospheric conductivity. Here we make use of this empirical relation for determining the conductivity distribution.

[12] Our SAPS events have been identified in the same way as described by *Wang et al.* [2008] in both hemispheres. It is a clearly identifiable sunward ion flow in the subauroral and premidnight region. A threshold of SAPS velocity greater than 100 m/s is used for selection. The

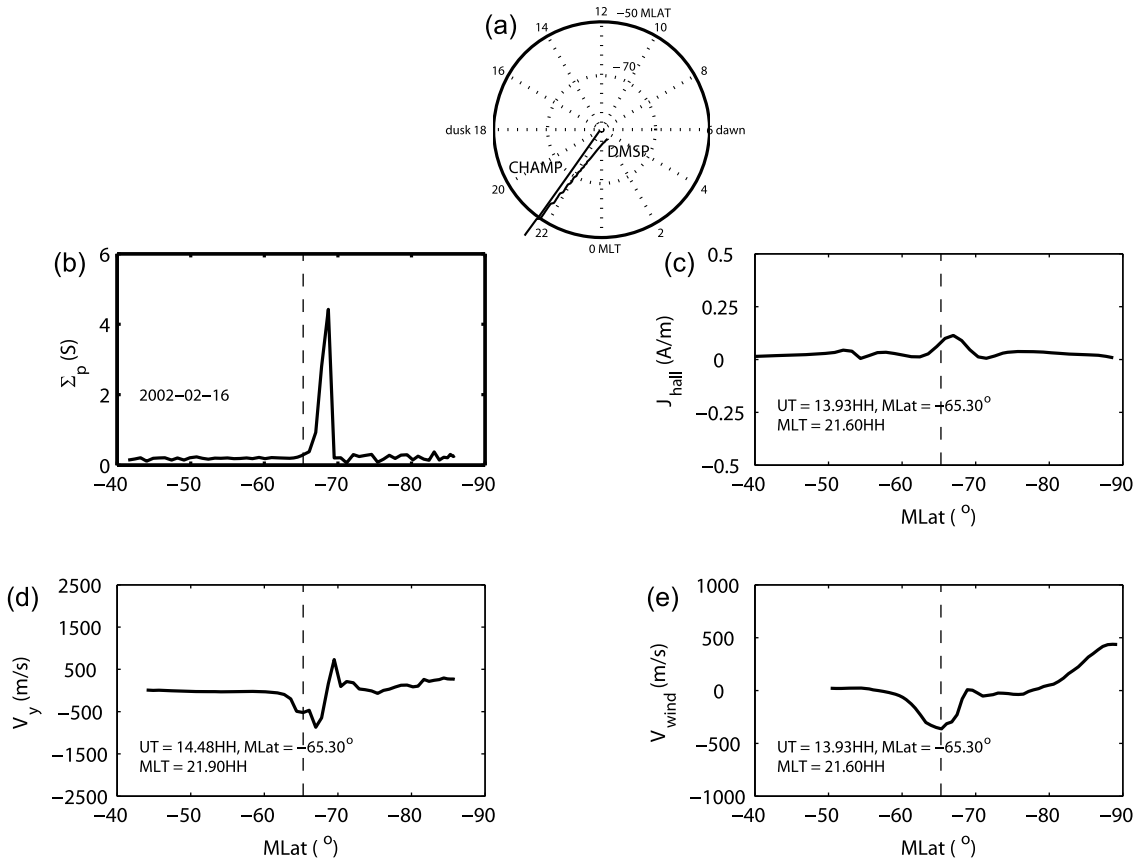

Figure 1. (a) CHAMP and DMSP Track in the ionosphere. Example of latitude profile of (b) Pedersen conductivity Σ_P, (c) plasma cross-track velocity V_y obtained from DMSP, (d) Hall current J_{Hall}, and (e) zonal wind speed V_{wind} from CHAMP. Positive marks eastward velocity and current. The peak velocity of westward SAPS is indicated by the dashed line. The UT, MLAT, and MLT where the SAPS velocity peaks are listed.

subauroral region is found automatically by computing the auroral Pedersen conductance along the DMSP path and determining the peak conductance, then stepping equatorward until the conductance is reduced to 0.2 times the peak value or 1 S, whichever is smaller. The selected orbits are further visually inspected to fully satisfy the above criteria. The universal time (UT), magnetic local time (MLT), magnetic latitude (MLat) and magnitude of the peak velocities of SAPS are recorded for each event. During 2002 and 2003 the SAPS events are observed generally during 1500–2200 MLT in the Northern Hemisphere and 1600–2400 MLT in the Southern Hemisphere. The MLT coverage difference is due to the larger offset between the geomagnetic pole and the geographic pole in the Southern Hemisphere than in the Northern.

[13] CHAMP and DMSP measurements in both hemispheres from the years 2002 and 2003 have been processed. There are altogether 1965/1790 close CHAMP and DMSP approaches during 2002 and 2003 in the Northern/Southern Hemisphere, respectively. A "close approach" requires that CHAMP passes the MLat of the peak velocity of SAPS within a zonal segment of ±15° in longitude and a time window of ±1 h of the SAPS detection time. As mentioned earlier, only CHAMP passes are considered where the angle between orbit and oval is larger than 45°.

[14] As an example, Figure 1 shows the latitudinal variation of electrodynamic parameters in the premidnight sector coordinately observed by CHAMP and DMSP over the southern middle-high latitude region. The upper plot shows the ionospheric polar footprints of CHAMP and DMSP. CHAMP comes from nightside toward dayside, while DMSP flies from dayside toward nightside. They have closely aligned orbit segments along the 2200 MLT meridian. CHAMP flies through the region about 30 minutes ahead of DMSP's detection of a SAPS peak. In Figure 1 we have plotted the latitude profile of the Pedersen conductivity derived from the particle precipitation (Figure 1b), ionospheric convection in the east–west direction (Figure 1d), Hall current (Figure 1c), and neutral wind (Figure 1e). Positive values represent eastward directions, that is antisunward direction in the dusk-premidnight sector. The conductivity and convection velocity on the left side are from DMSP and the current and wind on the right side are from CHAMP. The magnetic activity during the period is Kp = 1+ and $D_{ST} = -2$ nT.

[15] The obviously large conductivity due to particle precipitation at high latitudes between 65° and 70° MLat represents the quiet time auroral oval, and the sunward ion flow (westward, negative value) in this premidnight region is the auroral zone plasma convection. The enhanced westward plasma drift (negative) equatorward of the auroral

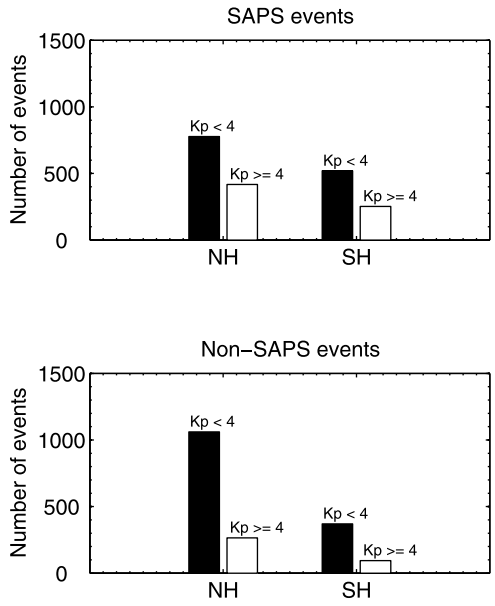

Figure 2. Number of selected collocated CHAMP and DMSP passes in both hemispheres for Kp < 4 and Kp ≥ 4 during periods (top) with SAPS and (bottom) without SAPS.

precipitation is the SAPS, whose peak velocity of −500 m/s is indicated by the vertical dashed line. This magnitude of SAPS velocity is typical for quiet period and increases with increasing magnetic activity [*Wang et al.*, 2008]. In Figure 1c, the positive (eastward) Hall current peak of 0.2 A/m occurs a little poleward of the SAPS peak, and a little equatorward of the conductivity peak. The Hall current strength is typical for the quiet condition. During magnetic storms the current can reach several A/m [*Ritter et al.*, 2004]. From Figure 1e, we see that the westward wind peak of about −400 m/s occurs around the SAPS peak. The subauroral wind is considerably stronger than the quiet time background wind of 100 m/s in the dusk auroral zone [*Lühr et al.*, 2007b]. The stronger zonal wind in the subauroral zone might be related to the SAPS, as suggested by *Lühr et al.* [2007b]. From this typical event it seems that the subauroral poleward polarization electric field can drive strong westward disturbance zonal winds in the subauroral region. In the nightside subauroral region the ion/electron density is low, compared to the auroral region, due to the devoid of particle precipitation. It is interesting that the low-density ions can have such great effects on the neutrals. In order to test the significance of these findings we have performed a statistical study, making use of all closely conjugated observations of CHAMP and DMSP.

3. Statistical Results

3.1. Number of Events

[16] The numbers of coordinated CHAMP-DMSP observations in both hemispheres are shown in Figure 2. Figure 2 (top) is for passes with SAPS events and the bottom is for passes without SAPS. The non-SAPS periods are studied for comparison to get the general features of electrodynamic parameters. For periods of non-SAPS, the close approach requires that CHAMP passes the peaks of plasma convection velocities within a zonal segment of ±15° in longitude and a time window of ±1 h around the time DMSP detected the plasma convection peaks. In total, there are 1194 (771) collocated CHAMP and DMSP orbits for SAPS (non-SAPS) periods in the Northern Hemisphere and 1326 (464) orbits in the Southern Hemisphere. We have further divided the events according to two geomagnetic activities, with Kp < 4 for less disturbed and Kp ≥ 4 for active periods. Due to the difference in geometry between geomagnetic pole and geographic pole the events in the south are fewer than in the north. The events during Kp ≥ 4 are much fewer in the Southern than in the Northern Hemisphere, which is due to the 45° threshold selection criterion for CHAMP orbits. We have more than 200 events in every activity bin, except for non-SAPS events during Kp ≥ 4 in the south pole (~100). Due to this low sample number and the high activity the average curves from that bin, as described in section 3.3, are not so smooth and so reliable. The event numbers, in general, can be regarded sufficient for a statical study. The following investigations will be performed separately for each bin. The results of the plasma velocity, current and wind velocity are all ordered in the frame of corrected magnetic coordinates and magnetic local times, which are both calculated from the Apex algorithm [*Richmond*, 1995].

3.2. SAPS Periods

[17] In order to obtain the internal relationship between SAPS, ionospheric Hall current, and neutral wind, we have performed a superposed epoch analysis (SEA). We take the peak SAPS location as key MLat, and DMSP and CHAMP latitude profiles are staged, centered on that key point. Then the mean velocity and density profiles can be obtained with 1° MLat resolution. We examine the variations from 30° equatorward of SAPS peaks to 20° poleward of SAPS peaks.

[18] Figure 3 shows the average dynamics of cross-track plasma velocities observed by DMSP for quiet and disturbed periods in both hemispheres. Figures 3a–3d are from the Northern Hemisphere and Figures 3e–3h are from the Southern Hemisphere. In Figure 3 (left) the observations for Kp < 4 and in Figure 3 (right) the observations for Kp ≥ 4 are shown. Figures 3a, 3b, 3e, and 3f are the stack plots of DMSP velocities presented and Figures 3c, 3d, 3g, and 3h are the SEA analysis of them. Later currents and winds are presented in the same format.

[19] In Figure 3 all curves show fast westward flows at the key latitude, which are SAPS features. When averaged over all orbits, the peak westward flow occurs at the zero latitude. The averaged SAPS velocity reaches −960/−1240 m/s during Kp ≥ 4 and −710/780 m/s during Kp < 4 in the Northern/Southern Hemisphere, respectively (as listed in Table 1). With more geomagnetic activity SAPS become larger in magnitude and wider in the MLat coverage. The plasma convection becomes eastward in the polar cap. The SAPS in the Southern Hemisphere are larger than in the Northern.

[20] We show in Figure 4 the occurrence distribution of SAPS peaks as a function of MLat for both geomagnetic activity conditions. SAPS tend to shift equatorward when the geomagnetic activity increases. The most likely location tends to occur at 64°–68°/62°–64° MLat for Kp < 4 and 60°/58°–60° MLat for Kp ≥ 4 in the Northern/Southern Hemisphere, respectively.

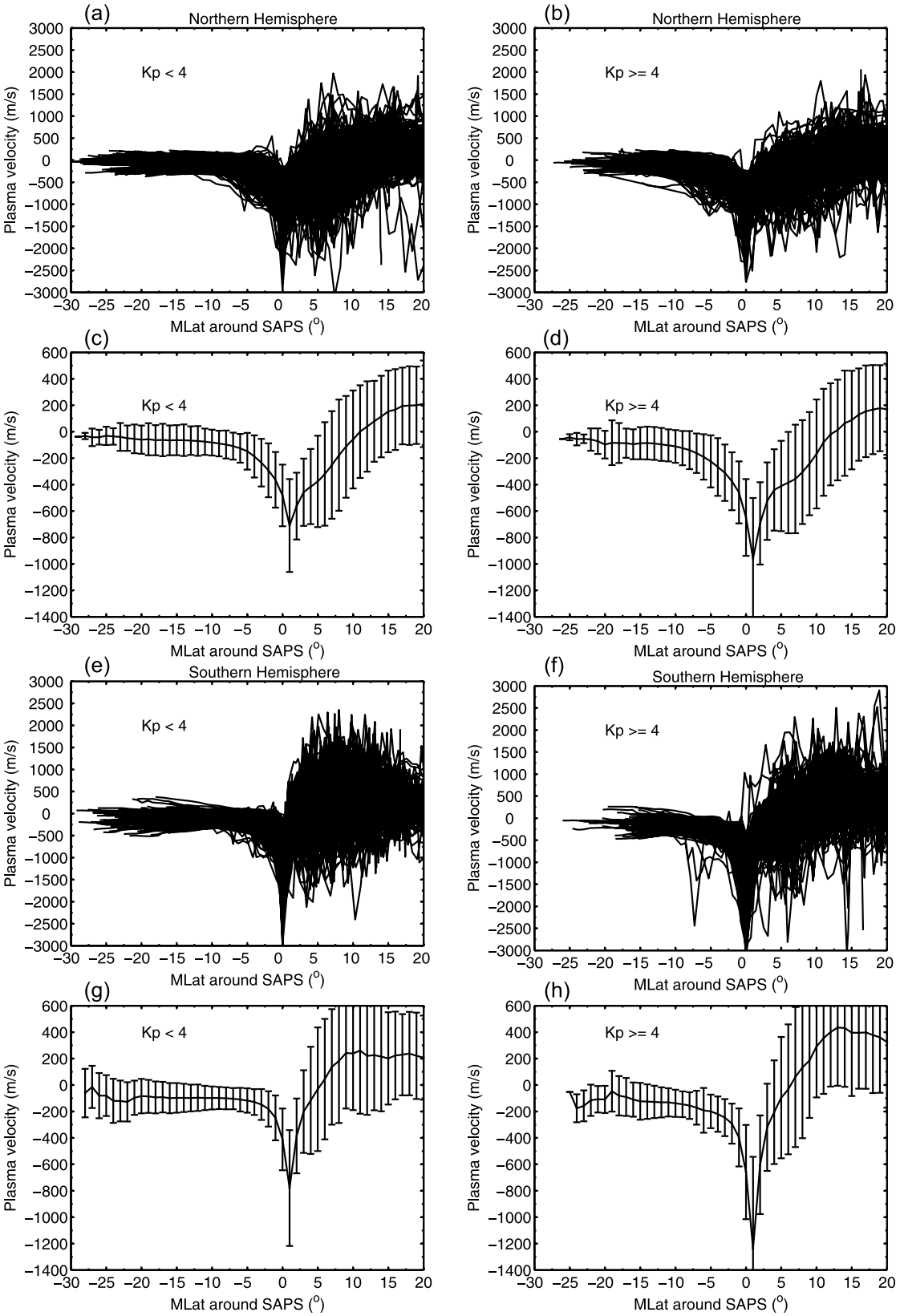

Figure 3. (a, b, e, and f) Stack plots and (c, d, g, and h) superposed epoch analysis of the cross-track velocity observed by DMSP in both hemispheres for Kp < 4 and Kp ≥ 4. The key MLat of "0" denotes MLat where SAPS peak occurs. Positive denotes eastward velocity. The bars show the standard deviations of 1° averages.

Table 1. Characteristics Like Peak Amplitude and MLat of Plasma Drift, Hall Current, and Wind Velocity During SAPS Events

	Northern Hemisphere				Southern Hemisphere			
	Kp < 4		Kp ≥ 4		Kp < 4		Kp ≥ 4	
	ΔMLat(°)	Peak	ΔMLat(°)	Peak	ΔMLat(°)	Peak	ΔMLat(°)	Peak
Plasma drift (m/s)	0.0	−710	0.0	−960	0.0	−780	0.0	−1240
Hall current (mA/m)	1.5	140	1.5	150	1.0	50	1.5	50
Wind (m/s)	0.5	−215	0.0	−242	0.0	−80	0.0	−118

[21] The latitude variation of Hall current density during these SAPS periods are shown in Figure 5. It is presented in the same format as Figure 3. All curves show a bipolar variation of Hall current, with eastward currents equatorward and the westward currents poleward, which is typical for the dusk-premidnight sectors. The current strength is larger and the width is wider during disturbed periods than during relatively quiet periods. The averaged Hall currents peak poleward of the zero latitude, which is valid in both hemispheres. To seek the peaks of eastward Hall current more precisely, we have fitted a fourth-order polynomial to the averaged curves between −4° and 4° MLat. It is found that the eastward Hall current peaks are located at 1.5°/1.0° with a magnitude of 0.14/0.05 A/m during Kp < 4 and at 1.5°/1.5° with a magnitude of 0.15/0.05 A/m during Kp ≥ 4 in the Northern/Southern Hemisphere, respectively (for details see Table 1).

[22] Figure 6 shows the average latitude distribution of zonal wind along orbits during these SAPS periods. Equatorward of the key latitude we observe prevailing eastward winds of about 80–100 m/s on the nightside. They decrease gradually in magnitude with increasing MLat and switch to westward wind at about −10°, and peak around zero latitude. Then they recover and become eastward again about 10° poleward of the key latitude. Through the fourth-order polynomial fitting to the averaged curves, we get the peak westward wind velocities of −215/−80 m/s during Kp < 4 and −242/−118 m/s during Kp ≥ 4 in the Northern/Southern Hemisphere, respectively (as listed in Table 1). The westward wind is stronger and wider in latitude coverage during Kp ≥ 4 than during Kp < 4. These tendencies are the same in both hemispheres. The difference of the peak velocity of wind and SAPS at 0°, as listed in Table 1, have been further validated by a t test in order to see whether the difference is statistically significant. The t test shows that the wind and plasma velocities in the 0° MLat bin have totally different mean values, with the absolute velocity difference being 456–526/632–732 m/s for Kp < 4 and 620–776/991–1256 m/s for Kp ≥ 4 in the Northern/Southern Hemisphere, respectively. The test provides confidence that the averaged values are statistically significant.

[23] The SAPS are larger in the Southern Hemisphere than in the Northern Hemisphere, but the associated winds in the Southern Hemisphere are smaller in magnitude than those in the Northern Hemisphere. A possible explanation for this effect will be offered in section 4.

3.3. Non-SAPS Periods

[24] In a next step we want to get the general wind distribution in the dusk-premidnight sector as a function of MLat. We consider now passes without SAPS for both hemispheres and for Kp < 4 and Kp ≥ 4. We take readings from 30°–80° MLat and stack the observations from DMSP and CHAMP.

[25] Figure 7 shows the average plasma velocity observed by DMSP for Kp < 4 and Kp ≥ 4 in both hemispheres during non-SAPS periods. It can be seen that the westward (sunward) plasma convection covers regions around 60°–75° MLat for Kp < 4. It shifts equatorward and becomes wider around 55°–75° MLat for Kp ≥ 4. The peak magnitudes are −324/−223 m/s at 69.0°/66.0° MLat for Kp < 4 and −409/−301 m/s at 65.5°/60.5° MLat for Kp ≥ 4 in the Northern/Southern Hemisphere, respectively (as listed in Table 2). The plasma velocity increases with geomagnetic activity. When comparing Figure 7 to Figure 4, it can be seen that SAPS peak equatorward of auroral plasma flow peaks, which is quite reasonable.

[26] Figure 8 shows the latitudinal distribution of Hall currents during non-SAPS times. All curves of Hall currents exhibit typical bipolar current pictures in the dusk sector, with eastward currents in the auroral zone and westward currents in the polar cap. The average eastward auroral Hall current strength is 0.08/0.06 A/m (0.13/0.04 A/m) for Kp < 4 (Kp ≥ 4) in the Northern/Southern Hemisphere, respectively. The average auroral zone center latitude can be determined from the peak eastward Hall current density,

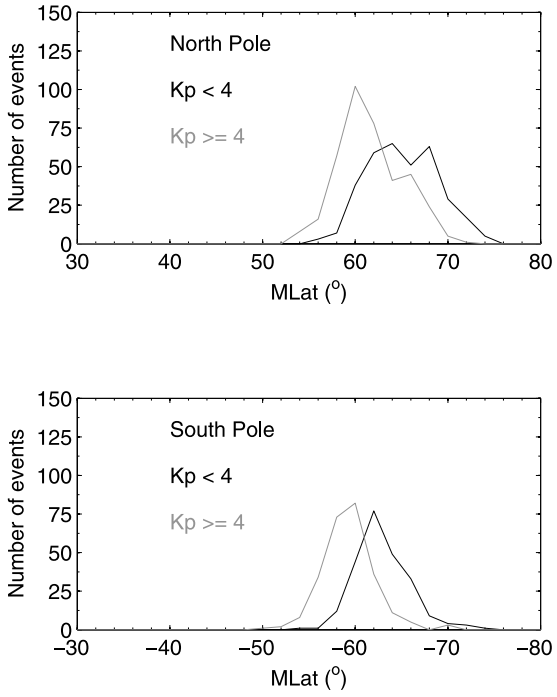

Figure 4. Occurrence distribution of SAPS events as a function of MLat for Kp < 4 and Kp ≥ 4 in both hemispheres.

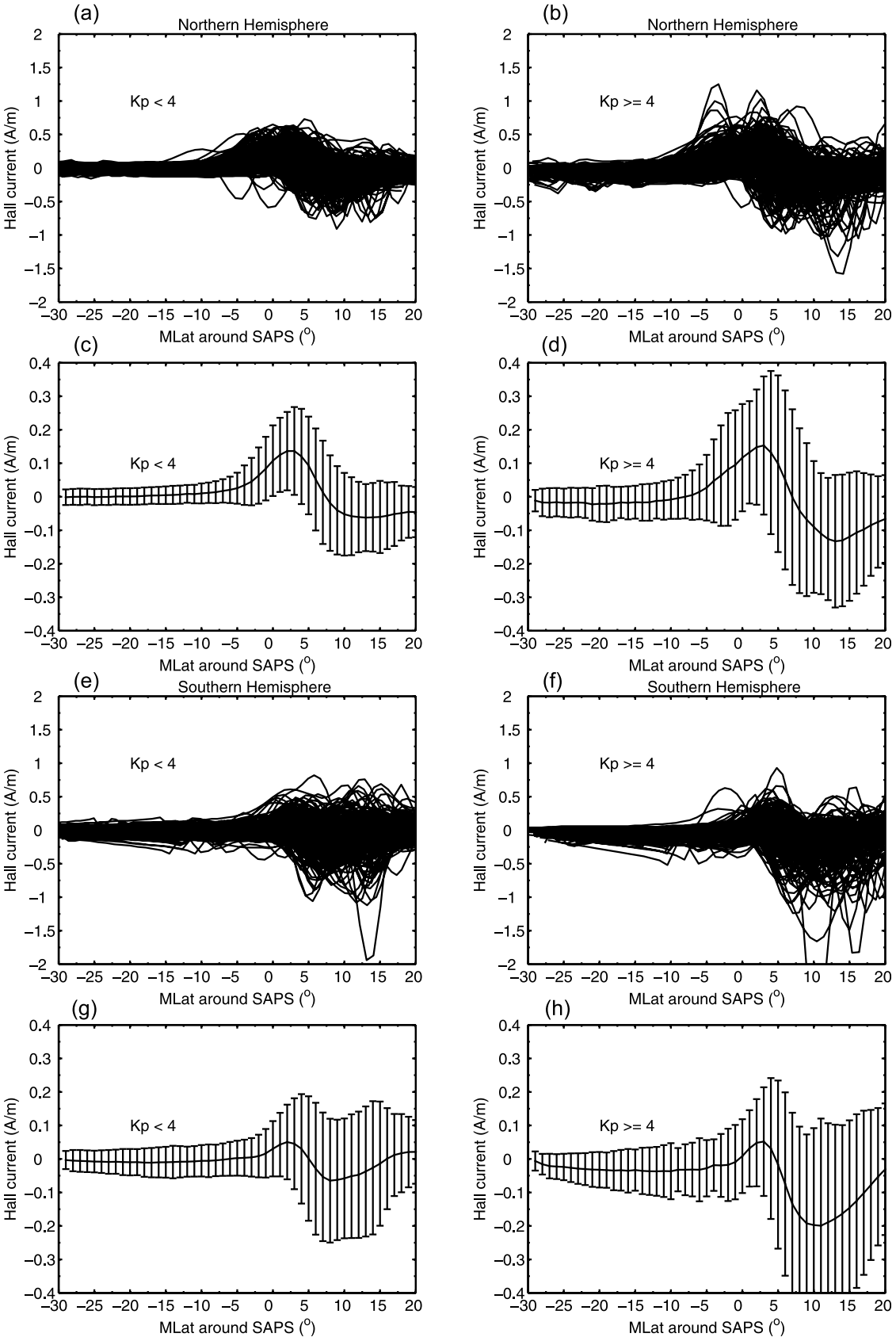

Figure 5. (a, b, e, and f) Stack plots and (c, d, g, and h) superposed epoch analysis of the Hall current density recorded by CHAMP in both hemispheres for Kp < 4 and Kp ≥ 4. The key MLat of 0 denotes MLat where the SAPS peak occurs. Positive denotes eastward Hall current.

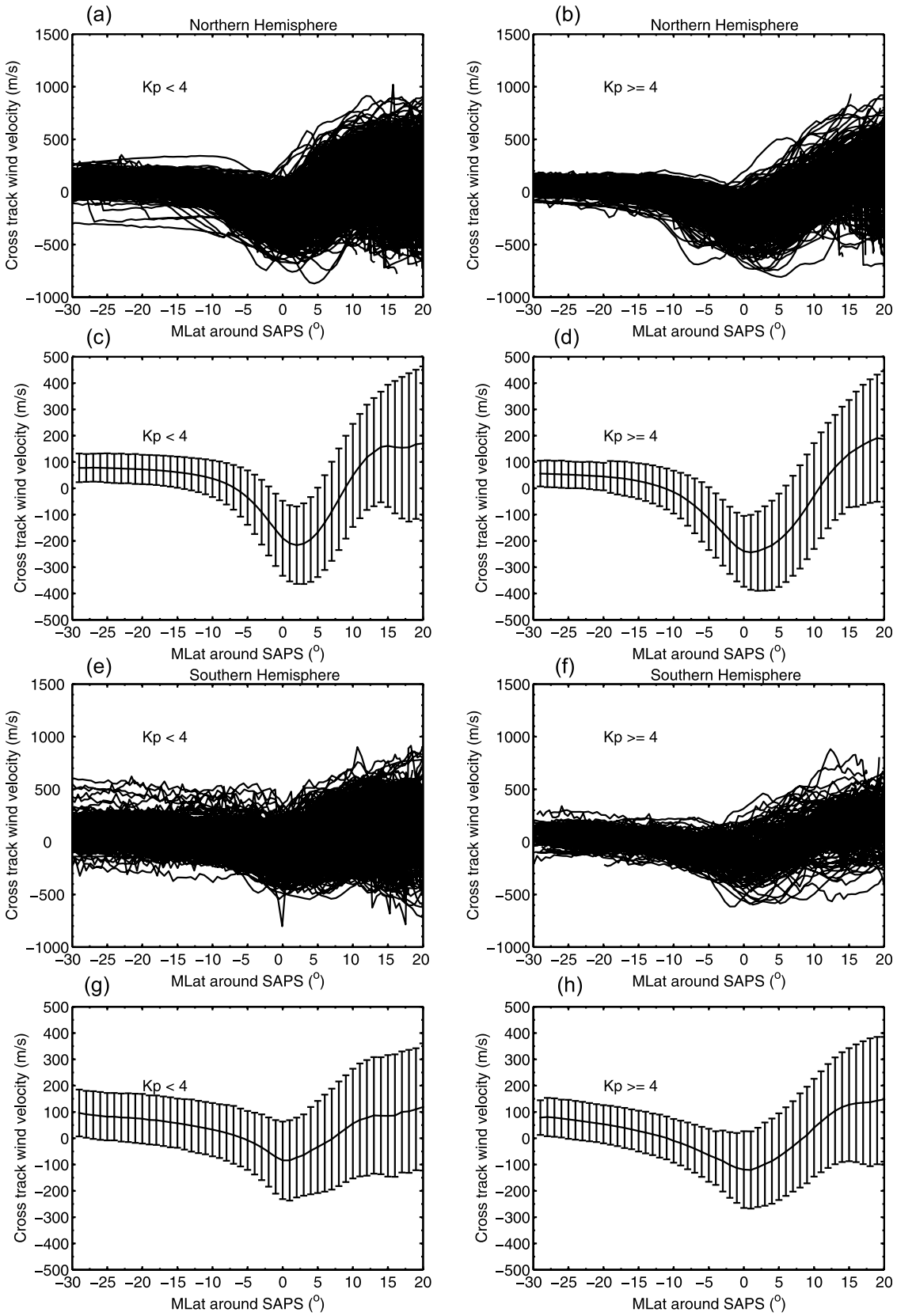

Figure 6. (a, b, e, and f) Stack plots and (c, d, g, and h) superposed epoch analysis of the cross-track wind observed by CHAMP in both hemispheres for Kp < 4 and Kp ≥ 4. The key MLat of 0 denotes MLat where the SAPS peak occurs. Positive denotes eastward wind velocity.

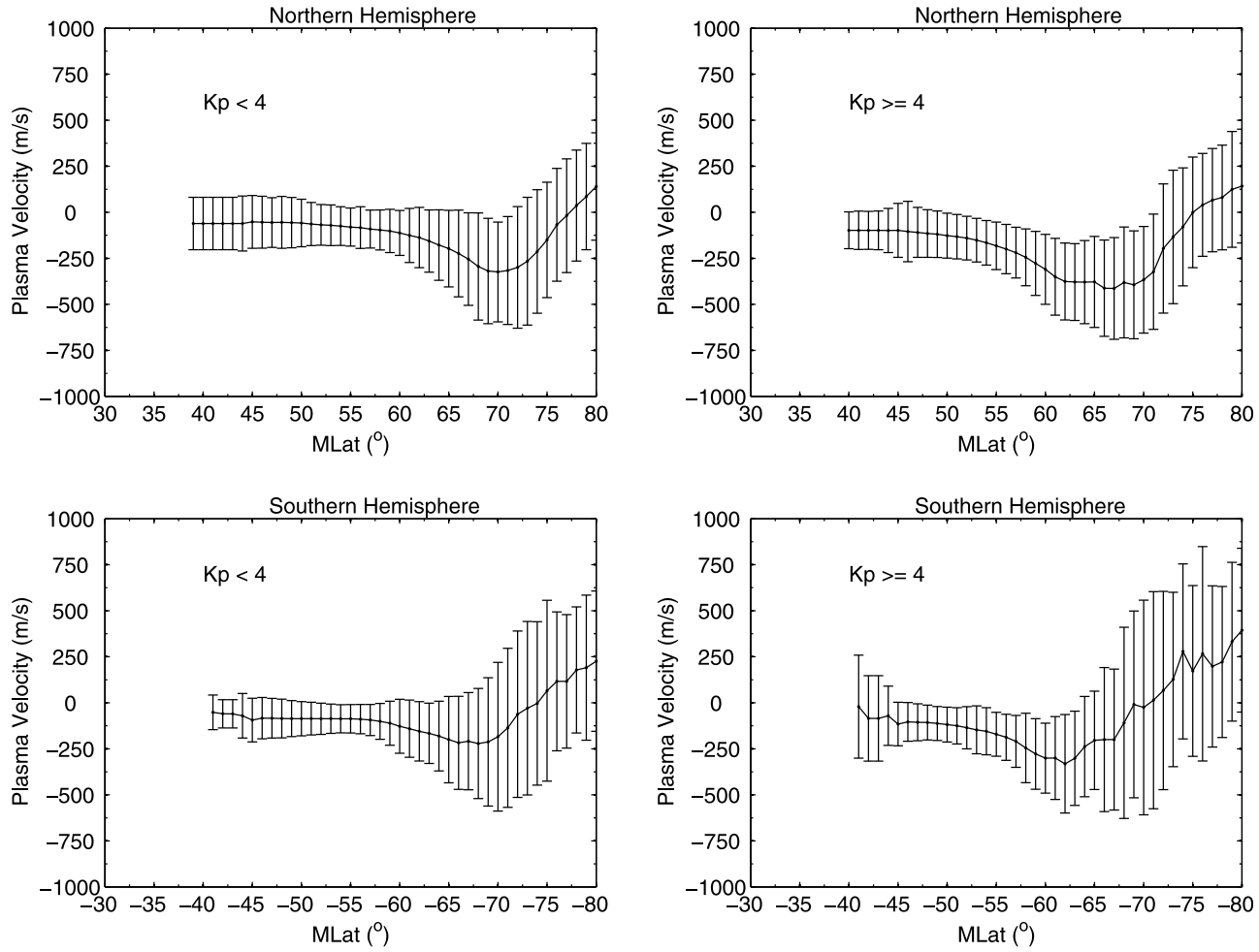

Figure 7. Superposed epoch analysis of the cross-track plasma velocity observed by DMSP for Kp < 4 and Kp ≥ 4 during non-SAPS periods in both hemispheres.

which is 67.5°/66.0° MLat (64.5°/58.5° MLat) for Kp < 4 (Kp ≥ 4) in the Northern/Southern Hemisphere, respectively. The numbers have been listed in Table 2.

[27] Figure 9 shows the latitudinal variation of the zonal wind during non-SAPS period. Steady eastward wind of around 50–100 m/s can be observed at mid latitudes in both hemispheres for both Kp < 4 and Kp ≥ 4. Strong westward wind can be found within the auroral zone. The average magnitude of the peak wind speed is −120/−79 m/s for Kp < 4 and −175/−88 m/s for Kp ≥ 4 in the Norhtern/Southern Hemisphere, respectively. The centers of peaks are 68.5°/67.5° MLat for Kp < 4 and 64.0°/59.0° MLat for Kp ≥ 4 in the Northern/Southern Hemisphere, respectively. The numbers are listed in Table 2. The westward wind velocity gets enhanced and the width gets wider with the geomagnetic activity. The southern auroral zone wind is weaker than the northern. The peak magnitude and location of the westward (sunward) wind is quite comparable with previous studies [e.g., *Thayer et al.*, 1987; *Lühr et al.*, 2007b].

4. Discussion

[28] In section 3, we have presented results of our statistical analysis about the influence of plasma drift on neutral wind at subauroral and auroral latitudes. The local time sector considered covers the hours from dusk to premidnight. An important finding is that there are differences between observations with and without SAPS events.

Table 2. Characteristics Like Peak Amplitude and MLat of Plasma Drift, Hall Current, and Wind Velocity During Non-SAPS Periods

	Northern Hemisphere				Southern Hemisphere			
	Kp < 4		Kp ≥ 4		Kp < 4		Kp ≥ 4	
	MLat(°)	Peak	MLat(°)	Peak	MLat(°)	Peak	MLat(°)	Peak
Plasma drift (m/s)	69.0	−324	65.5	−409	−66.0	−223	−59.0	−351
Hall current (mA/m)	67.5	80	64.5	130	−66.0	60	−58.5	40
Wind (m/s)	68.5	−120	64.0	−175	−67.5	−79	−59.0	−88

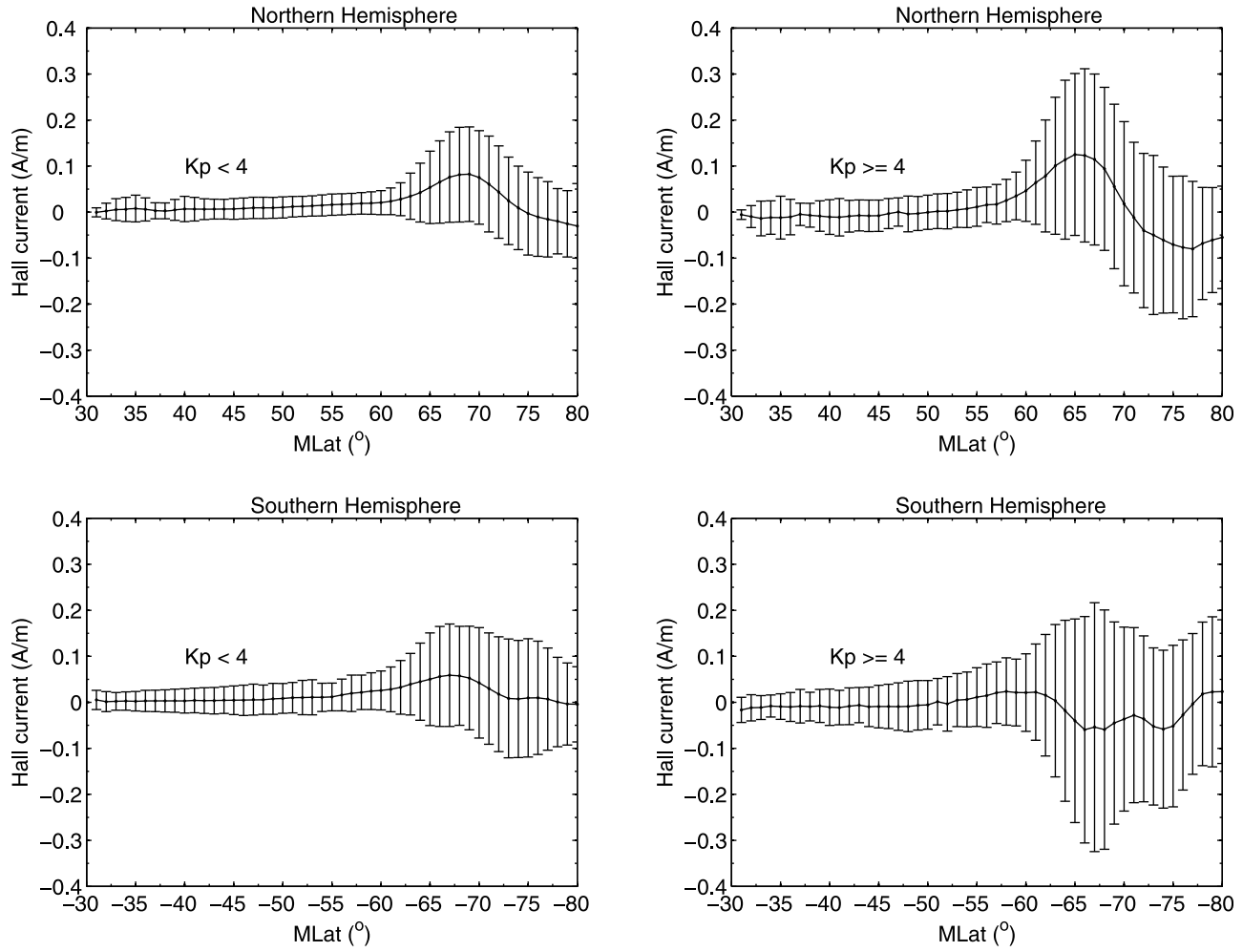

Figure 8. Superposed epoch analysis of the Hall current observed by DMSP for Kp < 4 and Kp ≥ 4 during non-SAPS periods in both hemispheres.

4.1. Characteristics of SAPS Events

[29] Before we focus on the thermospheric response to SAPS, we want to discuss some of the features resulting from our study. Quantitative results of the statistic analysis of SAPS and non-SAPS periods are listed in Table 1 and 2, respectively. Peak locations of the curves for plasma drift, wind and current density have been determined by fitting a degree 4 polynomial to the average curves around the maximum.

[30] During SAPS periods the plasma drift peaks by design at the key latitude, "0°". As expected, plasma drifts are higher during more active times. Interestingly, the velocities in the Southern Hemisphere are higher by 10–30% than in the Northern. This could be due to the seasonal dependence of the SAPS velocity. The SAPS velocity is inversely proportional to the subauroral ionospheric conductivity [e.g., *Wang et al.*, 2008]. The mid latitude trough, where the ion and electron density drop, can be very pronounced in winter and fall and less evident in summer and spring, owing to photoionization [*Schunk et al.*, 1976]. We have more local summer and spring events in the north (286 events in local summer and spring and 131 events in local winter and autumn for Kp ≥ 4) while a little more winter and fall events in the south (132 events in local winter and fall and 120 events in local summer and spring for Kp ≥ 4). Thus, one would expect larger subauroral conductivity in the north than in the south. The neutral wind is stronger in the north than in the south. The reason might be the ion drag force, which is proportional to both ion velocity and ion density, and the latter is larger in the north than in the south.

[31] In the subauroral region the ion density may play a more important role. During non-SAPS periods both the plasma and neutral velocity in the north are larger than those in the south, because we have larger auroral conductivity in the south than in the north (conductivity due to particle precipitation derived from DMSP measurement, figure not shown). This indicates that in the auroral region the plasma velocity plays a more important role in driving the neutrals since we have enough ion density. The neutral wind shows a clear geomagnetic activity dependence with larger velocity during more active periods. This is consistent with previous model studies predicting that the southward IMF B_z control of the neutral wind is specially evident in the dusk sectors, and that the auroral zone wind at F region altitudes increases greatly with an increasing southward IMF B_z, due to the increasing convection electric field [*Deng and Ridley*, 2006].

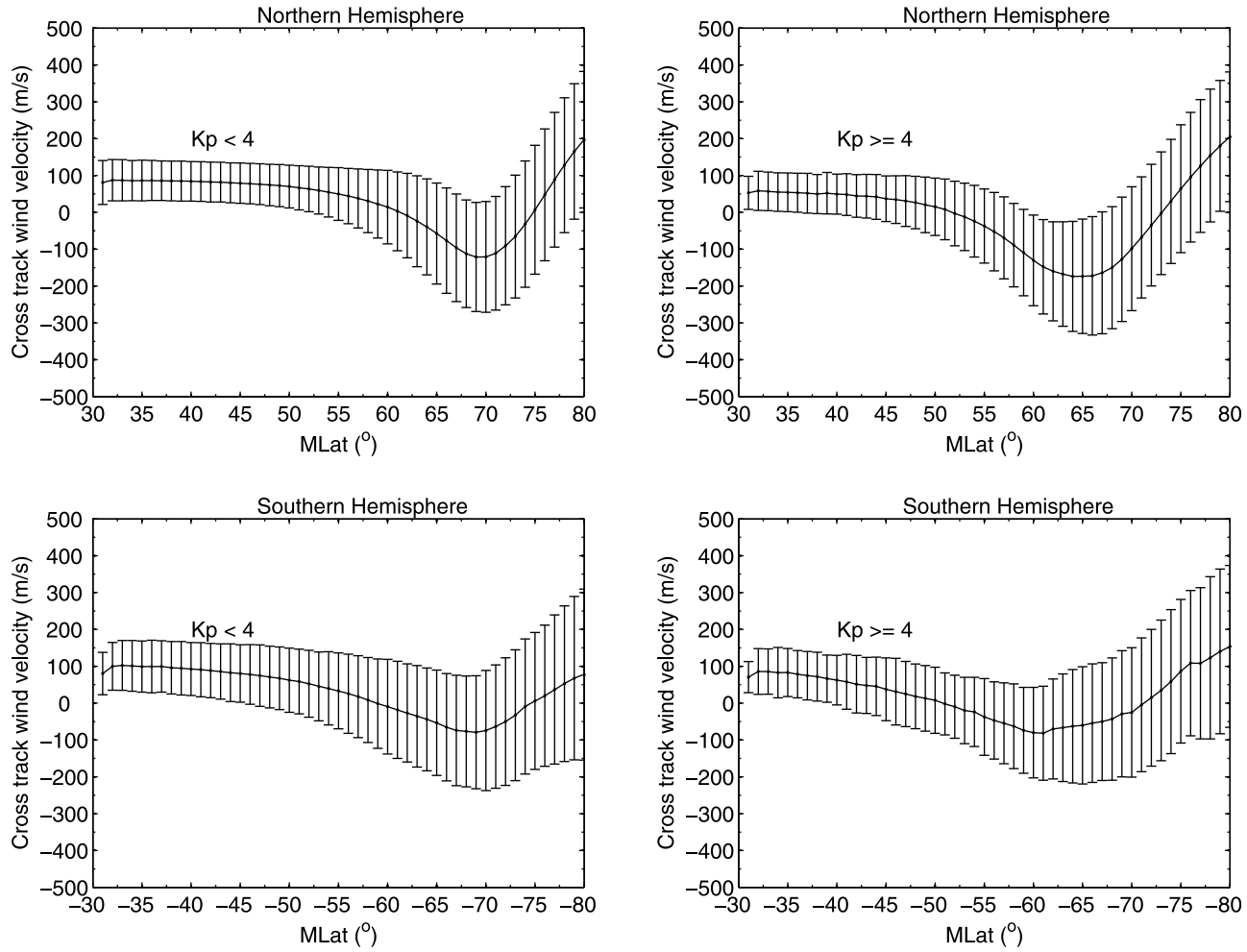

Figure 9. Superposed epoch analysis of the cross-track wind velocity observed by DMSP for Kp < 4 and Kp ≥ 4 during non-SAPS periods in both hemispheres.

[32] Neutral wind peaks at the same latitude as the SAPS, but the curve is somewhat broader than the plasma drift. This is expected since measurements have been taken by two different spacecraft and at some what different times. As a consequence the peak is more smeared out and the amplitude reduced. This effect is larger for high magnetic activity than for low, and it is more pronounced in the Southern than in the Northern Hemisphere. The difference in ratios in Table 1 between plasma velocity and wind for the four cases (e.g., both hemispheres and two levels of geomagnetic activities) can largely be explained by that effect. Support for that suggestion is provided by the ratios of plasma drift to wind velocity during non-SAPS periods (cf. Table 2). When averaging both quantities over latitude this ratio is more or less constant for all four cases, resulting in 2.75 ± 0.4 independent of the geomagnetic activity. Our result is consistent with previous model result [*Deng and Ridley*, 2006]. They found that the ratio between the neutral wind and the convection velocity showed little dependence on IMF B_z. We may probably assume a similar ratio between the plasma and neutral velocity for the SAPS events after excluding seasonal effects, when both quantities are measured by the same spacecraft such as the upcoming SWARM mission.

[33] The eastward Hall currents (auroral electrojet) peak at latitudes about 1.5° poleward of the SAPS drift. This is expected since the plasma jets flow at subauroral latitudes where the conductivity is reduced. Interestingly, the current density of the eastward electrojet does not show obvious increases with magnetic activity. However, the westward electrojet, located some 10° in latitude poleward does increase markedly. This behavior can be explained by the enhanced conductivity during higher magnetic activity.

[34] Close encounters of DMSP and CHAMP during non-SAPS periods have been used as control cases. The results compiled in Table 2 well confirm our findings about SAPS. During those periods westward plasma drifts peak again at the same latitude as the wind, but Hall currents (eastward electrojet) now peak, as expected, also at the same or even somewhat lower latitude. Previous model studies showed that the auroral hemispheric power has little effects on the neutral winds at 300 km altitude, and their effect is apparent below 170 km [*Deng and Ridley*, 2006]. The ionospheric currents (Joule heating) and particle precipitation are processes primarily confined to the low thermosphere region, thus their effect on neutral wind is modest at 400 km altitude. From the ratio current density over plasma drift we can estimate the mean conductivity. When assuming a magnetic

field strength of 40,000 nT at DMSP altitude we obtain Hall conductances of about 6.5 S and 8 S for the quiet and active periods. These numbers are very reasonable for the eastward electrojet region [e.g., *Schlegel*, 1988]. All these numbers provide confidence in the reliability of the measurements.

4.2. Influence of SAPS on Thermospheric Wind

[35] Generally, thermospheric winds are blowing from day to nightside due to the pressure gradient caused by the density and the neutral temperature difference. At F region altitudes the basic balance of forces is between ion drag and pressure, which is different from the E regions, where other forces like Coriolis and advection play significant roles [e.g., *Killeen and Roble*, 1984].

[36] During both SAPS and non-SAPS events (cf. Figures 3, 6, 7, and 9), it can be seen that at lower latitudes, equatorward of the auroral zone, the eastward neutral wind, V_n, is stronger than the almost stationary ion velocity, V_i. Thus, the ions exert a negative force to the neutrals. At subauroral and auroral latitudes this airflow driven by the pressure gradient is modified by plasma motion, and $V_i > V_n$ indicates that ions have a positive force on neutrals in the subauroral and auroral zone. Based on CHAMP wind measurements, *Lühr et al.* [2007b] have shown that there is a clear difference between the dawn and dusk side. While on the dawnside a day to night flow is observed through all latitudes, there is a reversal of the wind direction at auroral latitudes reported on the duskside. Wind data presented in Figures 6 and 9 confirm the dusk results. At mid latitude we find antisunward winds with 80–100 m/s velocity during less disturbed period (Kp < 4). During high activity it is somewhat lower, as expected. The wind direction switches to sunward at auroral latitudes or at the SAPS channel. In the polar cap strong winds are directed antisunward, which can be larger than the plasma convection velocity, indicating that the ion drag in the polar cap is sometimes a negative force [*Killeen and Roble*, 1984]. A possible reason is that the ion flow is in the same direction as the neutral pressure gradient in the polar cap. The combined forces can accelerate the neutral wind velocity to be larger than that of ions. Consequently, the ion drag force is a negative force on the neutral to balance the pressure gradient force [*Deng and Ridley*, 2006].

[37] The reversal of wind direction to sunward is clearly correlated with the plasma drift. Both peak at the same latitude regardless of SAPS occurrence. For non-SAPS events we have deduced an almost constant ratio between plasma drift and wind velocity (2.75). When applying that factor to the plasma drift peaks for SAPS, we obtain sunward wind velocity peaks of about 270 m/s (400 m/s) for Kp < 4 (Kp ≥ 4) conditions. These high wind speeds show that SAPS have a strong influence on the wind, clearly overriding all influences of the neutral drivers.

4.3. Heating by SAPS

[38] At auroral latitudes two important heating processes of the thermosphere are Joule heating and heating by ion-neutral friction. For the periods studied we have all the quantities observed, which are needed for quantifying their relative importance. As a response to heating the temperature will increase causing an expansion of the atmosphere. We expect thus a local enhancement of the air density, ρ, at the altitude of CHAMP.

[39] Joule heating is fulled by electric currents. It can be expressed as

$$P_j = \vec{j} \cdot \left(\vec{E} + \vec{u} \times \vec{B}\right) = \sigma_P E^{*2}, \quad (1)$$

where $\vec{j}$ is the current density, $\vec{E}$ is the electric field, $\vec{E}^* = \vec{E} + \vec{u} \times \vec{B}$ is the equivalent electric field, $\vec{u}$ is wind velocity, $\vec{B}$ is magnetic field, σ_P is the ionospheric Pedersen conductivity. Since σ_P generally peaks in the E layer, most of the heat will be deposited in the E region around 120 km altitude. Here the neutral mass density is fairly high, therefore the temperature is expected to rise only slightly. This may also applied for another possible heating source in the auroral zone E region like particle precipitation. Model results from *Deng and Ridley* [2006] showed that the precipitating heating only affects on the neutral wind at altitudes below 170 km. Previous model results also showed that the auroral heating sources probably cannot produce the changes at mid latitudes [*Fuller-Rowell et al.*, 1990].

[40] In case of frictional heating we can write as

$$P_k = n_e m_i \nu_{ni} (\vec{v} - \vec{u}) \cdot \vec{v}, \quad (2)$$

where n_e is the electron density, m_i the mean ion mass, ν_{ni} the collision frequency between ions and neutrals, $\vec{v}$ is the plasma velocity vector and $\vec{u}$ the neutral wind vector. Here it is assumed that vertical (field aligned) velocities are negligible. It can be seen that the heating power increases with the square of the plasma velocity at high drift speeds. For that reason it is expected that frictional heating plays an important role during SAPS events.

[41] The ion neutral friction can cause a large enhancement of ion temperature. Consequently, the O^+ will convert into NO^+ due to fast chemical reactions with increasing ion temperature and the subsequent fast dissociative recombination with electrons. Model results show that large westward drifts of 3 km/s imposed at 60° MLat can enhance ion temperature over 3000 K at the F region and decrease O^+ density [e.g., *Moffett et al.*, 1992]. Model results have shown that the frictional heating resulting from the ion-neutral temperature difference is very important in the SAPS region when compared to other heating sources [*Pintér et al.*, 2006].

[42] As a measure for the amount of thermospheric heating we take the change in mass density as observed by CHAMP. The approach of retrieving mass density from accelerometer readings is described by *Doornbos et al.* [2010]. Before averaging over the relevant passes the densities have been normalized to the mean height of 400 km in order to avoid the influences of changing orbital altitudes. Mass densities have been stacked in the same way as the other quantities.

[43] Figure 10 shows for the Northern Hemisphere the average mass density distribution during SAPS and non-SAPS events. Figures 10a, 10b, 10e, and 10f present the total density and Figures 10c, 10d, 10g, and 10h present the densities anomaly, $\Delta\rho$, after subtraction of a trend line. At first we may note that the background density is higher by about 10% during SAPS periods. This is valid for both activity levels. Another interesting feature is the formation of a density bulge at or slightly equatorward of the key latitude during SAPS. This can be regarded as an indication

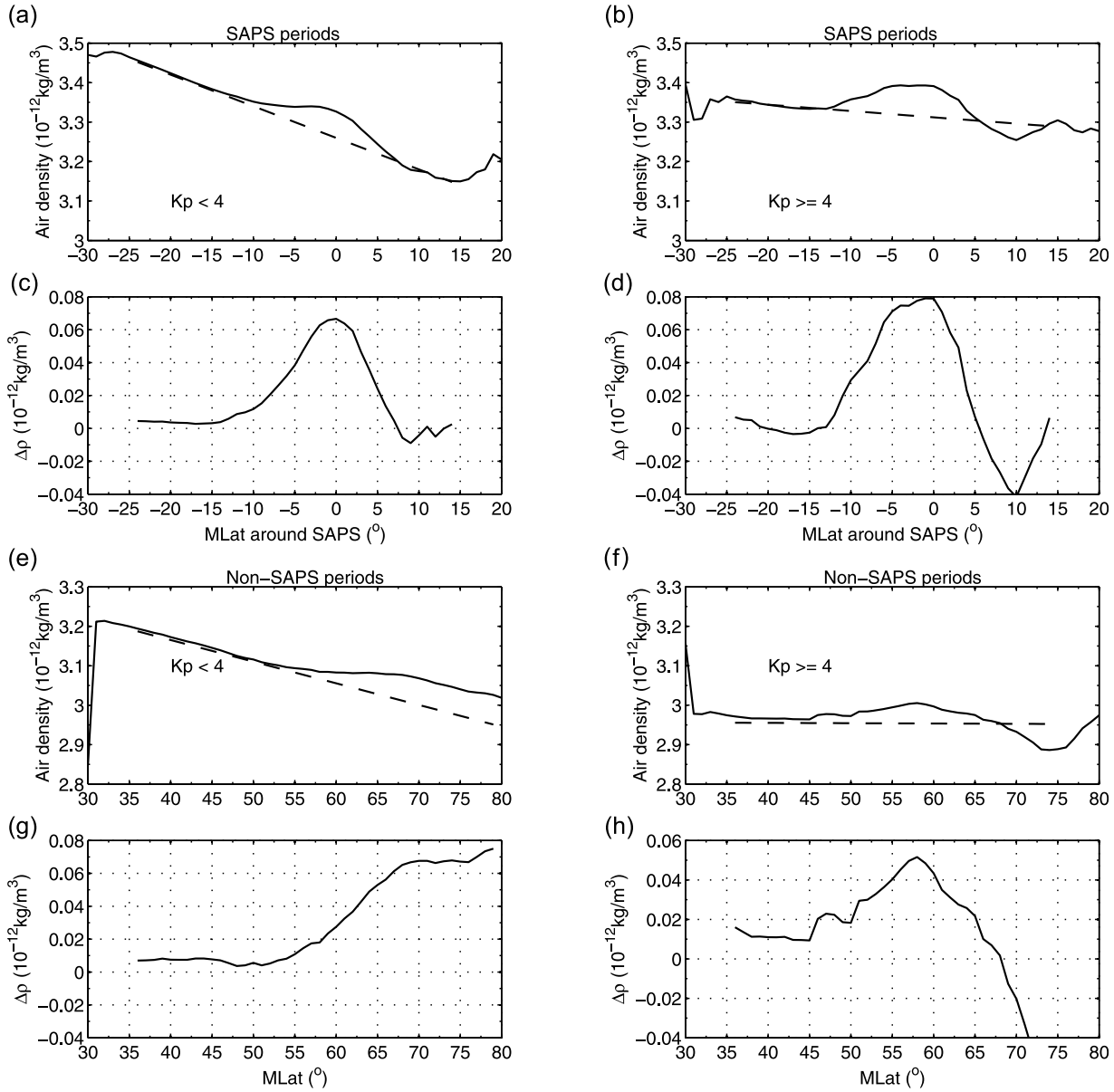

Figure 10. Average latitude profiles of thermospheric mass density at 400 km altitude. In the top Density profiles are shown from (a, b, e, and f) SAPS events and (c, d, g, and h) non-SAPS events. For both cases the total density for two levels of magnetic activity are presented. The dashed line is the trend line of the air density. Below the density anomalies, after subtraction of background density, is depicted. The mean standard deviations of the density are 1.37 and 1.33 × 10^{-12} kg/m^3 for Kp < 4 and 1.34 and 1.11 × 10^{-12} kg/m^3 for Kp ≥ 4 for SAPS and non-SAPS events, repectively.

of the dominance of frictional heating during SAPS events. Joule heating is expected to maximize at higher latitudes, where the currents peak.

[44] During non-SAPS times density anomalies appear at latitudes quite unrelated to the peaks in plasma drift and electrojet current. Previous statistical studies also revealed an area of enhanced air density in the premidnight sector between 50° and 72°, which becomes more prominent during more active periods [*Liu et al.*, 2005]. The air density maxima does not really agree with the maximal Hall currents [*Schlegel et al.*, 2005]. Possible reasons can be the dynamic responses of the thermosphere to local heating. *Ritter et al.* [2010] investigated the thermospheric response to magnetospheric substorms. They reported an equatorward motion of the density bulge created at onset as traveling atmospheric disturbance (TAD). The observations during SAPS events are synchronized in time and space. Therefore a more confined density response is expected. In case of the other periods observations take place at a random time offset to the activity enhancement. TADs thus had variable times to redistribute the density.

[45] Our observations clearly show that SAPS are efficient in heating the thermosphere in the dusk and premidnight sector. From the location of the density anomaly we conclude that frictional heating is the dominant process for causing density variations at 400 km altitude. Responses in

the Southern Hemisphere (not shown here) are similar as in the Northern Hemisphere but less pronounced.

5. Summary

[46] We have presented the first statistical study about the thermospheric response at 400 km altitude to subauroral polarization streams. Separate evaluations for SAPS occurring during moderate disturbed (Kp < 4) and magnetically active periods (Kp ≥ 4) have been performed. With the help of a superposed epoch analysis concurrent variations of related quantities are studied. As key latitude the peak in sunward plasma drift was chosen. For comparison mean latitude profiles of Hall current density (electrojet), zonal wind and mass density have been stacked in the same way as the plasma drift. In this way we revealed some characteristic features.

[47] 1. SAPS have a remarkable effect on the thermospheric wind. Strong sunward winds peak at the same latitude as the plasma drift. Wind speed reaches about 35% of the plasma velocity. During active periods the plasma velocity is about 45% higher.

[48] 2.The eastward electrojet peaks 1.5° MLat poleward of the plasma drift. This confirms the formation of SAPS equatorward of the high-conductivity channel. The eastward electrojet does not intensify with magnetic activity, but the westward electrojet becomes markedly stronger during disturbed periods.

[49] 3. The thermospheric mass density at 400 km altitude is enhanced during SAPS events by almost 10%. A density anomaly peak forms right at the latitude where the plasma drift maximizes. We regard this as an indication that frictional heating, caused by the motion of ions through neutral air, as the main process for modifying the density.

[50] For reference, the same analysis was performed for periods without SAPS events, again dividing the observations into two activity classes. Here we obtain the following results.

[51] 4. The zonal wind at auroral latitudes is again closely controlled by the plasma drift. Wind speeds are on average by a factor of 2.75 slower than the plasma velocity. Peak wind velocities are low during non-SAPS periods. In the Northern Hemisphere they reach only 60% of that during SAPS.

[52] 5. During non-SAPS periods the eastward electrojet peaks at almost the same latitude or somewhat equatorward of the sunward plasma drift. This confirms the difference in conductivity distribution.

[53] 6. The thermospheric density is lower during non-SAPS periods. There is no density anomaly directly related to current density or plasma drift peaks.

[54] Result obtained in the Northern Hemisphere have also be found in the Southern Hemisphere. Due to the larger offset between geographic and geomagnetic pole the sampling geometry is less favorable and with that the retrieved signature less clear.

[55] **Acknowledgments.** The operational support of the CHAMP mission by the German Aerospace Center (DLR) and the financial support for the data processing by the Federal Ministry of Education (BMBF), as part of the Geotechnology Programme, are gratefully acknowledged. We thank the Center for Space Sciences at the University of Texas at Dallas and the US Air Force for providing the DMSP IDM plasma data and the Space Physics Interactive Data Resource (SPIDR) for providing the DMSP SSJ/4 data. The WDC C2 for Geomagnetism at Kyoto are greatly acknowledged for providing the geomagnetic indices data. This work is supported by National Nature Science Foundation of China (40604017 and 40974096), National Basic Research Program of China (973 Program, 2011CB811404), open project founding of the State Key Laboratory of Space Weather of Chinese Academy of Sciences, the Scientific Research Foundation for the Returned Overseas Chinese Scholars, State Education Ministry, and the Fundamental Research Funds for the Central Universities.

[56] Robert Lysak thanks Asgeir Brekke and another reviewer for their assistance in evaluating this manuscript.

References

Anderson, P. C., R. A. Heelis, and W. B. Hanson (1991), The ionospheric signatures of rapid subauroral ion drifts, *J. Geophys. Res.*, *96*(A4), 5785–5792, doi:10.1029/90JA02651.

Anderson, P. C., W. B. Hanson, R. A. Heelis, J. D. Craven, D. N. Baker, and L. A. Frank (1993), A proposed production model of rapid subauroral ion drifts and their relationship to substorm evolution, *J. Geophys. Res.*, *98*(A4), 6069–6078, doi:10.1029/92JA01975.

Anderson, P. C., D. L. Carpenter, K. Tsuruda, T. Mukai, and F. J. Rich (2001), Multisatellite observations of rapid subauroral ion drifts (SAID), *J. Geophys. Res.*, *106*(A12), 29,585–29,600, doi:10.1029/2001JA000128.

Banks, P. M. (1972), Magnetospheric processes and the behavior of the neutral atmosphere, *Space Res.*, *12*, 1051–1067.

Brekke, A., J. R. Doupnik, and P. M. Banks (1974), Incoherent scatter measurements of E region conductivities and currents in the auroral zone, *J. Geophys. Res.*, *79*(25), 3773–3790, doi:10.1029/JA079i025p03773.

Brekke, A., S. Nozawa, and T. Sparr (1994), Studies of the E region neutral wind in the quiet auroral ionosphere, *J. Geophys. Res.*, *99*(A5), 8801–8825, doi:10.1029/93JA03232.

Burke, W. J., N. C. Maynard, M. P. Hagan, R. A. Wolf, G. R. Wilson, L. C. Gentile, M. S. Gussenhoven, C. Y. Huang, T. W. Garner, and F. J. Rich (1998), Electrodynamics of the inner magnetosphere observed in the dusk sector by CRRES and DMSP during the magnetic storm of June 4–6, 1991, *J. Geophys. Res.*, *103*(A12), 29,399–29,418, doi:10.1029/98JA02197.

Coley, W. R., R. A. Heelis, and N. W. Spencer (1994), Comparison of low-latitude ion and neutral zonal drifts using DE 2 data, *J. Geophys. Res.*, *99*(a1), 341–348, doi:10.1029/93JA02205.

Deng, Y., and A. J. Ridley (2006), Dependence of neutral winds on convection E-field, solar EUV, and auroral particle precipitation at high latitudes, *J. Geophys. Res.*, *111*, A09306, doi:10.1029/2005JA011368.

Doornbos, E., J. can den Ijssel, H. Lühr, M. Förster, and G. Koppenwallner (2010), Neutral density and crosswind determination from arbitrarily oriented multiaxis accelerometers on Satellites, *J. Spacecr. Rockets*, *47*, 580–589, doi:10.2514/1.48114.

Emmert, J. T., B. G. Fejer, C. G. Fesen, G. G. Shepherd, and B. H. Solheim (2001), Climatology of middle- and low-latitude daytime F region disturbance neutral winds measured by Wind Imaging Interferometer (WINDII), *J. Geophys. Res.*, *106*(A11), 24,701–24,712, doi:10.1029/2000JA000372.

Emmert, J. T., G. Hernandez, M. J. Jarvis, R. J. Niciejewski, D. P. Sipler, and S. Vennerstrom (2006), Climatologies of nighttime upper thermospheric winds measured by ground-based Fabry-Perot interferometers during geomagnetically quiet conditions: 2. High-latitude circulation and interplanetary magnetic field dependence, *J. Geophys. Res.*, *111*, A12303, doi:10.1029/2006JA011949.

Fejer, B. G., and L. Scherliess (1998), Mid- and low-latitude prompt-penetration ionospheric zonal plasma drifts, *Geophys. Res. Lett.*, *25*(16), 3071–3074, doi:10.1029/98GL02325.

Fejer, B. G., J. T. Emmert, and D. P. Sipler (2002), Climatology and storm time dependence of nighttime thermospheric neutral winds over Millstone Hill, *J. Geophys. Res.*, *107*(A5), 1052, doi:10.1029/2001JA000300.

Foster, J. C., and W. J. Burke (2002), SAPS: A new categorization for sub-auroral electric fields, *EOS Trans. AGU*, *83*(36), 393, doi:10.1029/2002EO000289.

Foster, J. C., and H. B. Vo (2002), Average characteristics and activity dependence of the subauroral polarization stream, *J. Geophys. Res.*, *107*(A12), 1475, doi:10.1029/2002JA009409.

Fuller-Rowell, T. J., D. Rees, B. A. Tinsley, H. Rishbeth, A. S. Rodger, and S. Quegan (1990), Modeling the response of the thermosphere and ionosphere to geomagnetic storms: Effects of a mid-latitude heat source, *Adv. Space Res.*, *10*, 215–223.

Galperin, Y., V. N. Ponomarev, and A. G. Zosimova (1974), Plasma convection in the polar ionosphere, *Ann. Geophys.*, *30*, 1–7.

Hardy, D. A., L. K. Schmitt, M. S. Gussenhoven, F. J. Marshall, and H. C. Yeh (1984), Precipitating electron and ion detectors (SSJ/4) for the block 5D/Flights 6-10 DMSP (Defense Meteorological Satellite Program) satellites: Calibration and data presentation, *Rep. AFGL-TR-84-0314*, Air Force Geophys. Lab., Hanscom AFB, Mass.

Häusler, K., H. Lühr, S. Rentz, and W. Köhler (2007), A statistical analysis of longitudinal dependences of upper thermospheric zonal winds at dip equator latitudes derived from CHAMP, *J. Atmos. Sol. Terr. Phys.*, *69*, 1419–1430, doi:10.1016/j.jastp.2007.04.004.

Hedin, A. E., E. L. Fleming, A. H. Manson, F. J. Schmidlin, S. K. Avery, R. R. Clark, S. J. Franke, G. J. Fraser, T. Tsuda, F. Vial, and R. A. Vincent (1996), Empirical wind model for the upper, middle and lower atmosphere, *J. Atmos. Terr. Phys.*, *58*, 1421–1447.

Heelis, R. A., and W. R. Coley (1992), East–west ion drifts at mid-latitudes observed by Dynamics Explorer 2, *J. Geophys. Res.*, *97*(A12), 19,461–19,469, doi:10.1029/92JA01840.

Killeen, T. L., and R. Roble (1984), An analysis of the high-latitude thermospheric wind pattern calculated by a thermospheric general circulation model: 1. Momentum forcing, *J. Geophys. Res.*, *89*(A9), 7509–7522, doi:10.1029/JA089iA09p07509.

Liemohn, M. W., A. J. Ridley, P. C. Brandt, D. L. Gallagher, J. U. Kozyra, D. M. Ober, D. G. Mitchell, E. C. Roelof, and R. DeMajistre (2005), Parametric analysis of nightside conductance effects on inner magnetospheric dynamics for the 17 April 2002 storm, *J. Geophys. Res.*, *110*, A12S22, doi:10.1029/2005JA011109.

Liu, H., H. Lühr, V. Henize, and W. Köhler (2005), Global distribution of the thermospheric total mass density derived from CHAMP, *J. Geophys. Res.*, *110*, A04301, doi:10.1029/2004JA010741.

Liu, H., H. Lühr, S. Watanabe, W. Köhler, V. Henize, and P. Visser (2006), Zonal winds in the equatorial upper thermosphere: Decomposing the solar flux, geomagnetic activity, and seasonal dependencies, *J. Geophys. Res.*, *111*, A07307, doi:10.1029/2005JA011415.

Lühr, H., K. Häusler, and C. Stolle (2007a), Longitudinal variation of F region electron density and thermospheric zonal wind caused by atmospheric tides, *Geophys. Res. Lett.*, *34*, L16102, doi:10.1029/2007GL030639.

Lühr, H., S. Rentz, P. Ritter, H. Liu, and K. Häusler (2007b), Average thermospheric wind patterns over the polar regions, as observed by CHAMP, *Ann. Geophys.*, *25*, 1093–1101.

McCormac, F. G., and R. W. Smith (1984), The influence of the Interplanetary magnetic field Y component on the ion and neutral motions in the polar thermosphere, *Geophys. Res. Lett.*, *11*(9), 935–938, doi:10.1029/GL011i009p00935.

Meriwether, J., M. Faivre, C. Fesen, P. Sherwood, and O. Veliz (2008), New results on equatorial thermospheric winds and the midnight temperature maximum, *Ann. Geophys.*, *26*, 447–466.

Moffett, R. J., R. A. Heelis, R. Sellek, and G. J. Bailey (1992), The temporal evolution of the ionospheric signatures of subauroral ion drifts, *Planet. Space Sci.*, *40*, 663–670, doi:10.1016/0032-0633(92)90007-B.

Moretto, T., N. Olsen, P. Ritter, and G. Lu (2002), Investigating the auroral electrojets with low altitude polar orbiting satellites, *Ann. Geophys.*, *20*, 1049–1061.

Olsen, N. (1996), A new tool for determining ionospheric currents from magnetic satellite data, *Geophys. Res. Lett.*, *23*(24), 3635–3638, doi:10.1029/96GL02896.

Pintér, B., S. D. Thom, R. Balthazor, H. Vo, and G. J. Bailey (2006), Modeling subauroral polarization streams equatorward of the plasmapause footprints, *J. Geophys. Res.*, *111*, A10306, doi:10.1029/2005JA011457.

Rees, D., T. J. Fuller-Rowell, R. Gordon, T. L. Killeen, P. B. Hays, L. Wharton, and W. Spencer (1983), A comparison of wind observations of the upper thermosphere from the Dynamics Explorer satellite with the predictions of a global time-dependent model, *Planet. Space Sci.*, *31*, 1299–1314, doi:10.1016/0032-0633(83)90067-3.

Reigber, C., H. Lühr, and P. Schwintzer (2002), CHAMP mission status, *Adv. Space Res.*, *30*, 129–134.

Rich, F. J., and M. Hairston (1994), Large-scale convection patterns observed by DMSP, *J. Geophys. Res.*, *99*(A3), 3827–3844, doi:10.1029/93JA03296.

Richmond, A. D. (1989), Modeling the ionosphere wind dynamo: A review, *Pure Appl. Geophys.*, *131*, 413–435, doi:10.1007/BF00876837.

Richmond, A. D. (1995), Ionospheric electrodynamics using magnetic apex coordinates, *J. Geomagn. Geoelectr.*, *47*, 191–212.

Richmond, A. D., C. Lathuillere, and S. Vennerstroem (2003), Wind in the high-latitude lower thermosphere: Dependence on the interplanetary magnetic field, *J. Geophys. Res.*, *108*(A2), 1066, doi:10.1029/2002JA009493.

Ridley, A. J., and M. W. Liemohn (2002), A model-derived storm time asymmetric ring current driven electric field description, *J. Geophys. Res.*, *107*(A8), 1151, doi:10.1029/2001JA000051.

Ritter, P., H. Lühr, A. Viljanen, O. Amm, A. Pulkkinen, and I. Sillanpää (2004), Ionospheric currents estimated simultaneously from CHAMP satellite and IMAGE ground-based magnetic field measurements: A statistical study at auroral latitudes, *Ann. Geophys.*, *22*, 417–430.

Ritter, P., H. Lühr, and E. Doornbos (2010), Substorm-related thermospheric density and wind disturbances derived from CHAMP observations, *Ann. Geophys.*, *28*, 1207–1220.

Robinson, R. M., R. R. Vondrak, K. Miller, T. Dabbs, and D. A. Hardy (1987), On calculating ionospheric conductances from the flux and energy of precipitating electrons, *J. Geophys. Res.*, *92*(A3), 2565–2569, doi:10.1029/JA092iA03p02565.

Rowland, D. E., and J. R. Wygant (1998), Dependence of the large-scale, inner magnetospheric electric field on geomagnetic activity, *J. Geophys. Res.*, *103*(A7), 14,959–14,964, doi:10.1029/97JA03524.

Scherliess, L., and B. G. Fejer (1998), Satellite studies of mid- and low-latitude ionospheric disturbance zonal plasma drifts, *Geophys. Res. Lett.*, *25*(9), 1503–1506, doi:10.1029/98GL01032.

Schlegel, K. (1988), Auroral zone E-region conductivities during solar minimum derived from EISCAT data, *Ann. Geophys.*, *6*, 129–138.

Schlegel, K., H. Lühr, J. Maurice, G. Crowley, and C. Hackert (2005), Thermospheric density structures over the polar regions observed with CHAMP, *Ann. Geophys.*, *23*, 1659–1672, doi:10.5194/angeo-23-1659-2005.

Schunk, R. W., P. M. Banks, and W. J. Raitt (1976), Effects of electric fields and other processes upon the nighttime high-latitude F layer, *J. Geophys. Res.*, *81*(19), 3271–3282, doi:10.1029/JA081i019p03271.

Smiddy, M., R. Sagalyn, B. Shuman, M. C. Kelley, W. Burke, F. Rich, R. Hays, and S. Lai (1977), Intense poleward-directed electric fields near the ionospheric projection of the plasmapause, *Geophys. Res. Lett.*, *4*(11), 543–546, doi:10.1029/GL004i011p00543.

Spiro, R. W., R. H. Heelis, and W. B. Hanson (1979), Rapid sub-auroral ion drifts observed by Atmospheric Explorer C, *Geophys. Res. Lett.*, *6*(8), 657–660, doi:10.1029/GL006i008p00657.

Thayer, J. P., T. L. Killeen, F. G. McCormac, C. R. Tschan, J. Ponthieu, and N. W. Spencer (1987), Thermospheric neutral wind signatures dependent on the east–west component of the interplanetary magnetic field for Northern and Southern Hemispheres as measured from Dynamics Explorer-2, *Ann. Geophys.*, *5*, 363–368.

Wang, H., H. Lühr, and S. Y. Ma (2005), Solar zenith angle and merging electric field control of field-aligned currents: A statistical study of the Southern Hemisphere, *J. Geophys. Res.*, *110*, A03306, doi:10.1029/2004JA010530.

Wang, H., A. J. Ridley, H. Lühr, M. W. Liemohn, and S. Y. Ma (2008), Statistical study of the subauroral polarization stream: Its dependence on the cross-polar cap potential and subauroral conductance, *J. Geophys. Res.*, *113*, A12311, doi:10.1029/2008JA013529.

Wygant, J., D. Rowland, H. J. Singer, M. Temerin, F. Mozer, and M. K. Hudson (1998), Experimental evidence on the role of the large spatial scale electric field in creating the ring current, *J. Geophys. Res.*, *103*(A12), 29,527–29,544, doi:10.1029/98JA01436.

Yeh, H.-C., J. C. Foster, F. J. Rich, and W. Swider (1991), Storm time electric field penetration observed at mid-latitude, *J. Geophys. Res.*, *96*(A4), 5707–5721, doi:10.1029/90JA02751.

Zhang, S. P., J. P. Thayer, R. G. Roble, J. E. Salah, G. G. Shepherd, L. P. Goncharenko, and Q. H. Zhou (2004), Latitudinal variations of neutral wind structures in the lower thermosphere for the March equinox period, *J. Atmos. Sol. Terr. Phys.*, *66*, 105–117, doi:10.1016/j.jastp.2003.09.011.

Zheng, Y., P. C. Brandt, A. T. Lui, and M. C. Fok (2008), On ionospheric trough conductance and subauroral polarization streams: simulation results, *J. Geophys. Res.*, *113*, A04209, doi:10.1029/2007JA012532.

K. Häusler, H. Lühr, and P. Ritter, Helmholtz Centre Potsdam, GFZ German Research Center for Geosciences, Telegrafenberg, D-14473 Potsdam, Germany.

H. Wang, Department of Space Physics, School of Electronic Informatics, Wuhan University, Hubei, Wuhan 430079, China. (h.wang@whu.edu.cn)